Stratigraphy around the Cretaceous-Paleogene boundary in sediment cores from the Lord Howe Rise, Southwest Pacific

Junichiro Kuroda[1,2], Kyoko Hagino[3], Yoichi Usui[2], Paul R. Bown[4], Kan-Hsi Hsiung[2], Saburo Sakai[2], Ron Hackney[5], Saneatsu Saito[2], Masafumi Murayama[3], Takuto Ando[6], and Naohiko Ohkouchi[2]

[1]Atmosphere and Ocean Research Institute, the University of Tokyo, 5-1-5 Kashiwanoha, Kashiwa, Chiba, 277-8564 Japan

[2]Japan Agency for Marine-Earth Science and Technology (JAMSTEC), 2-15 Natsushima-cho, Yokosuka, Kanagawa, 237-0061 Japan

[3]Center for Advanced Marine Core Research, Kochi University, 200 Monobe, Nankoku, Kochi, 783-0093 Japan

[4]Department of Earth Sciences, University College London, Gower Street, London WC1E 6BT, the United Kingdom

[5]Minerals, Energy, Groundwater Division, Geoscience Australia, GPO Box 378, Canberra ACT 2601, Australia

[6]Estuary Research Center, Shimane University, 1060 Nishikawatsu-cho, Matsue, Shimane 690-8504 Japan

ABSTRACT

During Deep Sea Drilling Project (DSDP) Leg 21, Cenozoic and latest Cretaceous sediments were recovered at Site 208 on the Lord Howe Rise, Southwest Pacific. We provide new biostratigraphic, magnetostratigraphic and chemostratigraphic data from Site 208 to constrain the stratigraphy around the Cretaceous-Paleogene (K-Pg) boundary and to determine

the depth of the K-Pg boundary more precisely. Biostratigraphic data from calcareous nannofossils indicate a near-continuous succession of sediments from the mid-Maastrichtian (Late Cretaceous) to lowermost Thanetian (Paleocene) at depths of 540-590 meters below seafloor (mbsf). The biostratigraphic data suggest that the K-Pg boundary corresponds to a siliceous claystone at the base of an interval of silicified sediments (576.0-576.8 mbsf). Carbonate carbon isotopic composition ($\delta^{13}C_{carb}$) reveals a negative shift across this interval, which is consistent with global patterns of $\delta^{13}C$ across the K-Pg boundary. Osmium concentration and Os isotopic composition ($^{187}Os/^{188}Os$) can also be used to identify the K-Pg boundary interval, as it is marked by a peak in Os concentration and a drop in $^{187}Os/^{188}Os$ values to 0.12-0.15, both of which are the result of the Chicxulub impact event. Our $^{187}Os/^{188}Os$ data show trends similar to those of coeval global seawater, with the lowest value of 0.12-0.16 in the siliceous claystone (576.8 mbsf). However, the concentration of Os is low (<80 pg g^{-1}) in this sample, which suggests that this siliceous claystone was deposited around the K-Pg boundary, but may not include the boundary itself. Although the sedimentary record across the K-Pg interval at Site 208 may not be completely continuous, it nevertheless captures a time interval that is close to the Chicxulub impact event.

INTRODUCTION

The Lord Howe Rise forms part of a large elongated strip of continental crust, which is called Zealandia (Crawford et al., 2003). During Deep Sea Drilling Project (DSDP) Leg 21, sediment cores were recovered at Site 208 on the northern portion of the Lord Howe Rise (Fig. 1) (The Shipboard Scientific Party et al., 1973). The recovered sediments are composed of a 488 m-thick sequence of calcareous ooze (late Pleistocene-late Oligocene, Unit 1), and a 106 m-thick sequence of nannofossil chalk and radiolarite (early middle Eocene-latest Cretaceous, Unit 2). A silicified interval, composed of silicified chalk and claystone, was recovered from 576.0 m below seafloor (mbsf) to 576.8 mbsf in Unit 2, which spans an interval across the Cretaceous-Paleogene (K-Pg) boundary (Edwards, 1973a).

The K-Pg boundary is characterized by an extraordinary mass extinction of terrestrial and marine biota. The trigger mechanism for the mass extinction was a large asteroid impact located on the Yucatan Peninsula, Mexico (i.e., Chicxulub impact event) (Alvarez et al., 1980; Schulte et al., 2010). The broader K-Pg interval also saw Deccan Traps volcanism on the Indian Subcontinent (Hull et al., 2020). Ravizza and Peucker-Ehrenbrink (2003) and Robinson et al. (2009) presented critical datasets of marine osmium isotopic records ($^{187}Os/^{188}Os$) from sediments of Maastrichtian age that show gradually declining values from ~0.6 to 0.4, starting around the magnetic chron boundary between C30n and C29r, which is about ~400 k.y. prior to the K-Pg boundary. The K-Pg boundary itself is marked by a sharp drop of $^{187}Os/^{188}Os$ values from 0.4 to 0.15, and then a return to ~0.4 in the earliest Paleocene (Ravizza and Peucker-Ehrenbrink, 2003; Robinson et al., 2009; Ravizza and VonderHaar, 2012). The gradual decrease and transient sharp drop have been attributed to increased weathering of basalts from the Deccan Traps and the Chicxulub impact event, respectively. These results suggest that the marine osmium isotopic records of the Upper Cretaceous to Paleocene have a distinct and resolvable shape that can be used as a robust chemostratigraphic tool to determine the relative timing of rapid and transient changes in osmium input to the oceans, and to assess the completeness of sedimentary successions (Ravizza and VonderHaar, 2012).

The circum-Australian region was located on the opposite side of the globe of the Chicxulub impact crater site (e.g., Müller et al., 2008; White et al., 2013) and should, therefore, have been less affected by the proximal effects of a large impact, such as mass wasting and/or tsunamis (e.g., Schulte et al., 2010). Marine sediments including the K-Pg boundary interval have been recovered in the circum-Australian basins and plateaus at Site 807C on the Ontong Java Plateau (Shipboard Scientific Party, 1991), Site 761C on the Wombat Plateau (Shipboard Scientific Party, 1990; Rocchia et al., 1992), Site 1172D in the Tasman Basin (Shipboard Scientific Party, 2001; Schellenberg et al., 2004), and Site U1514C in the Mentelle Basin (Huber et al., 2019), as well as Site 208 on the Lord Howe Rise (Fig. 1). Onshore, the K-Pg boundary has been identified in over 20 outcrop sections in New Zealand, some of which (e.g. bathyal Flaxbourne River section in the Marlborough sub-basin, Fig. 1) contain the most complete earliest Paleocene foraminiferal succession in the South Pacific (Hollis, 2003). Site 208 is therefore located in an area that is important for correlating the well-studied K-Pg sections in New Zealand with the other circum-Australian K-Pg sections.

Site 208 has arguably one of the best offshore sedimentary sections for examining the K-Pg boundary interval in the circum-Australian region. This is because the succession recovered from Site 1172D contains a major Danian hiatus and calcareous microfossils are poorly preserved. The K-Pg boundary section from Site 807C may be continuous, but calcareous microfossils are also poorly preserved around the K-Pg boundary interval because of the large burial depth of ~1200 mbsf (Shipboard Scientific Party, 1991). Given these deficiencies, a re-examination of biostratigraphic, magnetostratigraphic, and chemostratigraphic data at Site 208 allows better constraints to be placed on the nature of the K-Pg boundary in the Southwest Pacific. The results presented here will also complement new information from Site U1514C that shows a peak in platinum group elements (including osmium) and a decrease in $^{187}Os/^{188}Os$ (Ota et al., 2020); both of these conditions are evidence of the effects of the Chicxulub impact.

The original biostratigraphic study of Site 208 (The Shipboard Scientific Party et al., 1973; Edwards, 1973a) estimated the depth of the K-Pg boundary to be at 576.56 mbsf, about 30 cm above the lithologic change from calcareous nannofossil chalk to silicified sediment, the latter of which rarely yields calcareous nannofossils. The cause of the lithologic change and decline in abundance of calcareous nannofossils before the "estimated K-Pg section" is still unknown. To determine the level of the K-Pg boundary in this area more precisely, we carried out a complete re-examination of the calcareous nannofossil biostratigraphy for the Maastrichtian to Danian interval of Site 208 at higher stratigraphic resolution. In addition, we present new geochemical datasets of stable isotopic compositions of carbonate carbon ($\delta^{13}C_{carb}$), concentrations of osmium (Os), radiogenic isotopic compositions of osmium ($^{187}Os/^{188}Os$), and magnetic polarities for this section to test and support the biostratigraphic data. We also determined element abundances around the silicified interval using an X-ray fluorescence (XRF) core scanner to characterize the sediment geochemistry.

SAMPLES

Site 208 is located on the northern portion of the Lord Howe Rise (Fig. 1) at 26° 06.612' S, 161° 13.272' E and in a water depth of 1545 m (The Shipboard Scientific Party et al., 1973). A total of 34 cores were recovered with a rotary core barrel system, that penetrated to a depth of 594 m. Of the 306 m of the section that was cored, 255.4 m was recovered (83% recovery) but Core 208-32R was not recovered (567-576 mbsf).

The sediment succession was divided into two lithologic units. Unit 1 is a 488-m-thick sequence of calcareous ooze that spans the upper Oligocene to upper Pleistocene (0-488 mbsf). Unit 2 is a 106-m-thick sequence of siliceous fossil-bearing nannofossil chalk and nannofossil-bearing radiolarite that spans the Upper Cretaceous to lower middle Eocene (488-594 mbsf).

There are two major disconformities at Site 208: one at ~488 mbsf that separates Units 1 and 2 (between >40.4 Ma and <29.6 Ma), and the other at ~539 mbsf in Unit 2 that separates the middle Paleocene (>57.4 Ma) and middle Eocene (>47.8 Ma). A silicified interval, which is composed of silicified chalk and claystone, was recovered in the interval 576.0-576.8 mbsf (Section 208-33R-1, 0-83 cm). This silicified interval is characterized by less carbonate, more clay, and darker coloration than the underlying and overlying chalk. Edwards (1973b) provided a detailed lithological description of the boundary interval in Section 208-33R-1: from bottom to top, mid-Maastrichtian, light gray, bioturbated nannofossil chalk at 576.8-577.0 mbsf (82-101 cm of the section); Upper Maastrichtian, black to medium-gray, bioturbated cherty silicitite at 576.6-576.8 mbsf (56-82 cm); basal Danian, medium-gray, bioturbated silicitite at 576.3-576.6 mbsf (31-56 cm); and lower Danian, light-gray, bioturbated silicitite with black chert at 576.0-576.3 mbsf (0-31 cm). Based on calcareous nannofossil biostratigraphy, The Shipboard Scientific Party et al. (1973) and Edwards (1973a) suggested the presence of paraconformities at 576.82 mbsf, 576.56 mbsf, and 576.31 mbsf, and that the K-Pg boundary corresponds to one of the paraconformities at 576.56 mbsf (Section 208-33R-1, 56 cm). Based on radiolarian biostratigraphy, however, Hollis (1993) pointed out that the K-Pg boundary at Site 208 is located at the base of the silicified interval (576.8 mbsf). Because the approximate position of the K-Pg boundary was already constrained to be in Section 208-33R-1 (576.0-577.0 mbsf), we took 10-14 samples from Section 208-33R-1, and 1-10 samples from each section of Cores 208-33R (577.5-583.5 mbsf) and 208-34R (586.4-589.5 mbsf). We also took samples from Cores 208-29R (539.0-548.0 mbsf), 208-30R (548.0-557.0 mbsf), and 208-31R (559.0-562.5 mbsf) for calcareous nannofossil biostratigraphy and magnetostratigraphy.

ANALYTICAL METHODS

Calcareous Nannofossils

Standard smear slides were prepared for the study of calcareous nannofossils from 47 sediment samples collected from Sections 208-34R-3 to 208-29R-3 following Bown and Young (1998). Calcareous nannofossils were examined at 1500× magnification using a Nikon E600 cross-polarizing and phase contrast light microscope. Preservation of nannofossils in each sample was rated as follows: G = good: little or no evidence of dissolution and/or overgrowth, and specimens are identifiable at the species level; M = moderate: minor dissolution or crystal overgrowth is observed, but most specimens are identifiable to the species level; and, P = poor: strong dissolution or crystal overgrowth, and many specimens are unidentifiable at the species and/or generic level. The abundance of total calcareous nannofossils, as well as that of individual taxa was estimated as: A = abundant (11 or more specimens/field of view (FOV)), C = common (1 to 10 specimens/FOV), F = few (1 specimen/2 to 50 FOV), R = rare (1 specimen/51 or more FOV), and B = barren.

The calcareous nannofossil biostratigraphic scheme of Burnett (1998 – UC zones) was used in the Cretaceous interval, while Martini (1971 – NP zones) and Agnini et al. (2014 – CNP zones) were used for the Paleogene interval. The taxa considered in this study are listed in the Supplemental Material[1]. Bibliographic references for these taxa can be found in Bown (1998) and/or the online Nannotax database (http://ina.tmsoc.org/Nannotax3; accessed July 2021).

Stable Isotopic Composition of Carbonate Carbon ($\delta^{13}C_{carb}$)

The stable isotopic composition of bulk carbonate carbon ($\delta^{13}C_{carb}$) was determined at the Japan Agency for Marine-Earth Science and Technology (JAMSTEC) using an isotope ratio mass spectrometer (GV Instruments IsoPrime) with an automated carbonate reaction system (Multiprep). Isotopic ratios are reported with respect to the Vienna Pee Dee Belemnite (VPDB) standard using standard delta notation ($\delta^{13}C$) in permil. Analytical precision for the in-house carbonate standard was better than 0.06‰.

Re-Os Analysis

We extracted Re and Os from sediment samples using inverse aqua regia digestion. The detailed method for the extraction and separation of Re and Os is described by Tejada et al. (2009) and Kuroda et al. (2010). After spiking of ^{190}Os and ^{185}Re, ~1 g of powdered sample was sealed in a Carius tube (Shirey and Walker, 1995) with 4 ml of inverse aqua regia, and heated at 240°C for 24 hr. Os was then separated from the leachate using CCl_4 (Cohen and Waters, 1996; Pearson and Woodland, 2000) and further purified using the micro-distillation method (modified after Roy-Barman, 1993). Re was separated using a Bio-Rad AG1-X8 anion exchange resin (100-200 mesh).

Abundances and isotopic compositions of Os were analyzed by negative thermal ionization mass spectrometry (Thermo Fisher Scientific TRITON) at JAMSTEC, and abundances of Re were measured by an inductively coupled plasma-quadrupole mass spectrometer (Thermo Fisher Scientific iCAP-Q) at JAMSTEC. Total procedural blanks for Re and Os were 1.2-3 and 0.13-0.5 pg, respectively, with an average $^{187}Os/^{188}Os$ value of ~0.18 (n = 5). All data were corrected for the procedural blank for each analytical batch. Instrument reproducibility was monitored based on replicate analyses of the synthetic standard. Initial Os isotopic compositions ($^{187}Os/^{188}Os_i$) were calculated for the time of deposition based on the measured $^{187}Os/^{188}Os$ and $^{187}Re/^{188}Os$ values, the age of each sediment (DR1: Table S4), and the ^{187}Re decay constant of 1.666 (± 0.017) $\times 10^{-11}$ yr^{-1} (Smoliar et al., 1996). We calculated uncertainty in $^{187}Os/^{188}Os_i$ values using the sum of squared errors approach to propagate the uncertainties in the measured ^{187}Os/^{188}Os and ^{187}Re/^{188}Os ratios, and in the uncertainty of the ^{187}Re decay constant.

Paleomagnetism

We measured the natural remanent magnetization (NRM) of discrete samples at JAMSTEC. The samples were subjected to progressive alternating field (AF) demagnetization of up to 80 mT using the in-line demagnetizer and measured with the pass-through superconducting rock magnetometer (2G Enterprises Model 760). Results were analyzed by principal component analysis (PCA; Kirschvink, 1980) to isolate the characteristic remanent magnetization using the PuffinPlot software (version 1.03; Lurock and Wilson, 2012). Because samples were rotated independently around the vertical axis during Rotary Core Barrel coring, we only used inclination to define paleomagnetic polarity. We consider samples with near complete demagnetization and maximum angular dispersion (MAD) of less than 15° as robust.

X-Ray Fluorescence (XRF) Core Scanning

Relative abundances of elements (Al, Si, S, K, Ca, Ti, V, Mn, Fe, Ni, Cu, Zn, Br, Rb, Sr, Y, Zr and Ba) were analyzed for the split surface of Section 208-33R-1A by an ITRAX XRF core scanner (COX Analytical Systems, Croudace et al., 2006) at Kochi Core Center, Kochi University, Japan. Analysis was done using a Mo X-ray tube with settings of 30 kV, 55 mA and a 10-s measurement time (for detailed analytical conditions, see Seki et al., 2019 and Hsiung et al., 2021). Spatial resolution (step size of scanning) was 0.2 mm for the 52-65 cm interval of Section 208-33R-1A, and 1 mm for the other intervals.

RESULTS

Calcareous Nannofossil Biostratigraphy

A total of 46 out of 47 samples studied, collected between 589.33 mbsf and 543.17 mbsf, yielded Late Cretaceous and/or early Paleogene calcareous nannofossils (Figs. 2-4; DR1: Table S1, see footnote 1). Samples from the calcareous nannofossil chalk in 589.33-576.86 mbsf (from 208-34R-3, 130-133 cm to 208-33R-1, 86-90 cm) are characterized by well-preserved Maastrichtian taxa belonging to the genera *Arkhangelskiella*, *Cribrosphaera*, *Eiffellithus*, *Micula*, *Nephrolithus*, and *Prediscosphaera*. This interval is assigned to the Upper Maastrichtian Zone UC20c-d based on the occurrence of *Nephrolithus miniporus* (Burnett, 1998), although typical late Maastrichtian zonal marker taxa, such as *Micula prinsii*, *Ceratolithoides kamptneri*, and *Lithraphidites quadratus*, were not found (DR1: Table S1). The absence of these species in the Late Maastrichtian interval may reflect the nature of low diversity in calcareous nannoplankton in high latitudes of the southern hemisphere (Watkins et al., 1996; Burnett, 1998).

The bottom part of the silicified interval at 576.83-576.74 mbsf (from 208-33R-1, 80-83 cm to 208-33R-1, 74-77 cm) yielded rare Late Maastrichtian taxa, including K-Pg survivor taxa (DR1: Table S1). Preservation of the calcareous nannofossils in this interval was poor or moderate. It is uncertain whether the observed Cretaceous taxa are in situ or reworked from older sediments.

Calcareous nannofossil assemblages in the silicified interval between 576.74 mbsf and 576.17 mbsf (from 208-33R-1, 72-74 cm to 208-33R-1, 17-19 cm) consist of Late Maastrichtian, K-Pg survivor and early Danian taxa. The lower samples at 576.74-576.36 mbsf (208-33R-1, 72-74 cm to 208-33R-1, 36-38 cm) are assigned to the basal Danian Zone CNP1 (equivalent to NP1 of Martini, 1971) based on the occurrence of *Biantholithus sparsus* and absence of *Coccolithus pelagicus* (the marker species for Zone CNP2). The remaining upper two samples at 576.32-576.17 mbsf (208-33R-1, 30-32 cm and 17-19 cm:) from this interval are assigned to the Zone

CNP2 (equivalent to NP2 of Martini, 1971) based on the occurrences of *C. pelagicus* and the absence of taxa belonging to the *Prinsius dimorphosus* group (e.g. *Praeprinsius tenuiculus*), which defines the base of Zone CNP3. The Late Maastrichtian taxa observed in this interval include survivor and reworked forms.

Zone CNP3 (equivalent to NP3 of Martini, 1971) was identified between 562.43 mbsf and 561.10 mbsf (208-31R-3, 139-143 cm to 208-31R-3, 10-12 cm) based on the First Occurrence (FO) of *P. dimorphosus* and the absence of *Prinsius martini*.

The interval between 560.93 mbsf and 551.74 mbsf (from 208-31R-2, 140-143cm to 208-30R-3, 74-78 cm) is characterized by medium-sized *Prinsius* and *Toweius* taxa that diversified in the late Danian. Within this interval, the lower four samples within the interval 560.93-559.70 mbsf (from 208-31R-2, 140-143 cm to 21-208-31R-2, 20-22 cm) are assigned to the Zone CNP4 (equivalent to NP3-4 of Martini, 1971) based on the presence of *P. martini* and absence of *Toweius pertusus*. The upper four samples within the interval 556.72-551.74 mbsf (from 208-30R-6, 120-122 cm to 208-30R-3, 74-78 cm) are assigned to Zones CNP5-6 (equivalent to NP3-4 of Martini, 1971) based on the presence of *T. pertusus* and absence of *Lithoptychius* (=*Fasciculithus*) *ulii*. We are unable to differentiate between CNP Zones 5 and 6, as the marker taxa for CNP6 (*Sphenolithus moriformis*) was not found in this interval.

The Selandian Zone CNP7 (equivalent to NP4-5 of Martini, 1971) was identified between 550.73 mbsf and 545.84 mbsf (from 208-30R-2, 120-123 cm to 208-29R-5, 84-88 cm), based on the FO of *Lithoptychius ulii* and below the FO of *Heliolithus cantabriae*. A Sample from 540.62 mbsf to 540.60 mbsf (208-29R-2, 10-12 cm) was assigned to Thanetian Zone CNP8 (equivalent to NP6 of Martini, 1971) based on the presence of *Heliolithus cantabriae* and *Heliolithus kleinpellii* and the absence of *Discoaster mohleri*. Overall preservation of calcareous nannofossils in the Paleocene interval (CNP3 to CNP7) is good. Our revised calcareous nannofossil biostratigraphy in the Paleocene interval is basically consistent with that of The Shipboard Scientific Party et al. (1973) and Edwards (1973a,b), though the base of the NP5 Zone (FO of *Fasciculithus tympaniformis*) in this study is shallower than that of Edwards (1973a,b) (DR1: Fig. S2).

Chemostratigraphy of $\delta^{13}C_{carb}$

The $\delta^{13}C_{carb}$ values increase through the Upper Maastrichtian from +1.0‰ at 587.2 mbsf (208-34R-2, 73-76 cm) to +1.5‰ at 579.2 mbsf (208-33R-3, 17-19 cm), and then show a clear decrease from +1.4‰ at 577.6 mbsf (208-33R-2, 12-15 cm) to +0.33‰ at 576.4 mbsf (208-33R-1, 36-38 cm) (Fig. 3; DR1: Table S2). The $\delta^{13}C_{carb}$ values range between +0.75‰ and +1.5‰ in the Paleocene interval (Cores 208-31R to 208-29R), with some minor variations.

A negative shift of $\delta^{13}C_{carb}$ values across the K-Pg boundary has been widely recognized for the fine carbonate fraction or bulk carbonate, which shows positive values (generally between +1.5‰ and +3.0‰) in the uppermost Maastrichtian and then decreased values between 0‰ and +1.5‰ at the base of the Danian (D'Hondt, 1998; Coxall et al., 2006; Kroon et al., 2007; Schlte et al., 2010; Barnet et al., 2019; Hull et al., 2020). The clear negative shift of $\delta^{13}C_{carb}$ values at Site 208, with the initiation phase occurring around 576.8 mbsf (Fig. 4), correlates with the widely-recognized negative shift in $\delta^{13}C_{carb}$ across the K-Pg boundary. The $\delta^{13}C_{carb}$ trends across the K-Pg boundary at Site 208 are consistent with the calcareous nannofossil biostratigraphy (Figs. 3-4) supporting the placement of the K-Pg boundary at 576.8 mbsf (208-33R-1, 74-86 cm).

Magnetostratigraphy and Sedimentation Rates

Paleomagnetic polarity zones were constrained based on the magnetic polarity data (DR1: Table S3 and Fig. S1). Some samples from Sections 208-33R-1 and 208-33R-2 (576-579 mbsf) were not completely demagnetized by AF demagnetization at 80 mT (more than 30% of initial NRM remained). This indicates the presence of high coercivity minerals such as hematite. These samples are also characterized by NRM intensity 10-100 times larger than that of the other samples. Of these high coercivity samples, those with NRM decaying toward the origin were analyzed by PCA (note that those data are categorized as "data from incomplete demagnetization"; see legend of Fig. 2). For samples with NRM that does not decay toward the origin, we cannot exclude the possibility that they contain multi-polarity remanence components. In these cases we used the end-point polarity as "acceptable" data.

Chrons were assigned based on the geomagnetic polarity timescale (Ogg, 2020) using the calcareous nannofossil biostratigraphy (see Section "Calcareous Nannofossil Biostratigraphy" section). The paleomagnetic data suggest that the boundary between C30r and C30n (68.196 Ma) is located between 586.64 mbsf and 583.42 mbsf, and the boundary between C30n and C29r (66.398 Ma) is located between 579.67 mbsf and 578.55 mbsf (Figs. 2-3). Although the boundary between C29r and C29n (65.688 Ma) is unclear because the data show several reversals in the upper part of Section 208-33R-2 and the lower part of Section 208-33R-1 (577.62-576.90 mbsf), the C29r/C29n boundary should be located within this interval. The lack of Core 208-32R makes it difficult to constrain the positions of the paleomagnetic boundaries of C29n/C28r (64.958 Ma), C28r/C28n (64.677 Ma), and C28n/C27r (63.494 Ma). We assume that these boundaries lie within the unrecovered interval from 576 mbsf to 563 mbsf. In Core 208-30R, the boundaries of C27r/C27n (62.517 Ma) and C27n/C26r (62.221 Ma) occur within the intervals 556.70-551.78 mbsf and 551.74-549.04 mbsf, respectively (Fig. 2). The boundary between C26r and C26n (59.237 Ma) could be located between 549.01 mbsf and 542.69 mbsf.

The new calcareous nannofossil biostratigraphy and magnetostratigraphy are basically consistent and indicate a near-complete succession from the mid-Maastrichtian (Upper Cretaceous) to lowermost Thanetian (Paleocene). The age-depth plot based on these data gives a mean sedimentation rate of 3.8-4.9 m m.y.$^{-1}$ with clear decreases in sedimentation rate in Chrons C29r and C26r (Fig. 5). We speculate that the silicified interval in Section 208-33R-1, 0-83 cm, which includes the K-Pg boundary, was deposited at an even lower rate of sedimentation. Our paleomagnetic data indicate that the silicified interval lies within the paleomagnetic zone of C29n (Fig. 4), which is inconsistent with the widely accepted view that the K-Pg boundary occurred during C29r. This will be discussed later.

Re and Os Abundances and Os Isotopic Ratios ($^{187}Os/^{188}Os_i$)

Concentrations of Re and Os show a similar variation (Fig. 3) with low values in the Maastrichtian interval (576.9-589.3 mbsf), followed by higher values in the silicified interval (576.3-576.8 mbsf). The maximum values of Re (108 ng g^{-1}) and Os (581 pg g^{-1}) are seen at 576.58 mbsf (208-33R-1, 58 cm) (DR1: Table S4). Concentrations of Re and Os again decrease above this level.

Measured values of $^{187}Os/^{188}Os$ range between 0.42 and 2.5 (DR1: Table S4) with higher values seen around 576.5-576.6 mbsf in the silicified interval in Section 208-33R-1. Age-corrected initial values ($^{187}Os/^{188}Os_i$) range between 0.120 and 1.185 (DR1: Table S4). Most of the high values of measured $^{187}Os/^{188}Os$ were shifted to lower $^{187}Os/^{188}Os_i$ values by the age correction.

The $^{187}Os/^{188}Os_i$ values of sediment in the Maastrichtian interval (579-590 mbsf) range between 0.35 and 0.59, and the sediments between 576.8 and 579 mbsf have less radiogenic $^{187}Os/^{188}Os_i$ values of 0.28-0.44 (Fig. 3). A siliceous claystone sample from 576.8 mbsf (208-33R-1, 80-83 cm) has the minimum $^{187}Os/^{188}Os_i$ value of 0.12±0.4 and 0.16±0.4 (2 S.D., duplicate analysis) (Figs. 3-4). This sample has relatively high measured $^{187}Os/^{188}Os$ values (0.744-0.747), but high $^{187}Re/^{188}Os$ ratios (534-573) result in significant age correction. Sediments above this sample (576.7-576.2 mbsf) show higher $^{187}Os/^{188}Os_i$ values ranging between 0.27-0.59, with exceptionally high $^{187}Os/^{188}Os_i$ values of 1.19 and 0.91 at 576.58 mbsf (208-33R-1, 57.5-58 cm) and 576.52 mbsf (208-33R-1, 51-53 cm), respectively (Figs. 3 and 4).

XRF Core Scanning

The elemental abundances in Section 208-33R-1A determined by the XRF core scanner (Fig. 6), show a clear difference between the silicified interval from 576.0 mbsf to 576.8 mbsf (208-33R-1, 0-83 cm) and the underlying uppermost Maastrichtian chalk from 576.8 mbsf to 577.0 mbsf (208-33R-1, 83-101 cm). We could not analyze the siliceous claystone sample at 576.8 mbsf at the bottom of the silicified interval and the top of the section (576.0-576.1 mbsf) because the irregular surface of this sample was not suitable for XRF core scanning. Si is more abundant in the silicified interval (Fig. 6), which confirms the silicification in this interval. K, Ti, Fe and Rb, which are generally present within terrigenous clastic minerals such as illite, rutile and mica, are more abundant in the silicified interval (Fig. 6). Carbonate-associated elements such as Ca, Sr and Y are high in the chalk interval, and significantly decreased in the silicified interval (Fig. 6). In the silicified interval, Ca shows small peaks around 58-64 cm, where the presence of micrite was reported by Bralower et al. (2020). Sulfur shows similar variation with Ca, but S is also abundant in the 58-64 cm interval, where Ba and Fe are also high (Fig. 6). This suggests that sulfur is present mainly as carbonate-associated sulfate (CAS) in the chalk interval, but is present as barite and pyrite (and also as CAS) in the silicified interval. Our observation with a scanning electron microscope with energy dispersive X-ray spectroscopy (SEM-EDS) confirmed that both barite and pyrite are present in a sample from the interval 576.55-576.58 mbsf (208-33R-1, 55-58 cm). Mn is abundant in the chalk interval, which suggests the presence of Mn oxide or Mn carbonate in the chalk interval. Br intensity, which has been proposed as a tracer of marine organic matter (Seki et al. 2019), is slightly increased between 576.58 mbsf and 576.64 mbsf, which lies in the middle of the silicified interval. V, Ni, Cu and Zn are abundant in the silicified interval (Fig. 6). Al intensity is very low and noisy throughout the section because the Al Kα line is severely reduced during the measurement. Thus, we do not discuss the Al data any further.

DISCUSSION

Comparison of Os Isotopic Data with Global Trends

Osmium is nearly homogenized in the present-day ocean with an average residence time of 2-60 k.y. (e.g., Sharma et al., 1997; Burton et al., 1999; Levasseur et al., 1999; Peucker-Ehrenbrink and Ravizza, 2000; Oxburgh, 2001). Therefore, its isotopic composition is useful as a chemostratigraphic correlation tool (e.g., Ravizza and Peucker-Ehrenbrink, 2003; Robinson et al., 2009; Ravizza and VonderHaar, 2012; Hull et al., 2020). The composite marine Os isotopic record displays unique variation through the time period from Maastrichtian to Danian (the gray lines in Figs. 3-4). This includes: (1) marine $^{187}Os/^{188}Os$ values that are stable around 0.5-0.6 in Chron C30n during the Maastrichtian; (2) a gradual decrease in $^{187}Os/^{188}Os$ values to ~0.4 that is evident after the C30n/C29R boundary, followed by a stable phase at around 0.4 before the K-Pg boundary; (3) a transient sharp drop to ~0.12 at the K-Pg boundary, followed by quick recovery to 0.4 immediately after the K-Pg boundary, and (4) a stable phase of ~0.4 during the lowermost part of the Danian. A relatively longer-term supply of nonradiogenic Os from the Deccan Traps, starting from the C30n/C29r boundary, explains the drop of $^{187}Os/^{188}Os$ from 0.6 to 0.4 (2) and continuing through the Danian (4) (Ravizza and Peucker-Ehrenbrink, 2003; Robinson et al., 2009; Schoene et al., 2019). The very sharp drop in marine $^{187}Os/^{188}Os$ values (3) corresponds to the peak abundances of platinum group elements (Ru, Pd, Os, Ir, and Pt) at the K-Pg boundary, all of which are attributed to the Chicxulub impact event (Ravizza and Peucker-Ehrenbrink, 2003; Robinson et al., 2009; Ravizza and VonderHaar, 2012). The nonradiogenic Os supplied as a result of the impact event was quickly removed from the ocean after the impact (e.g., Ravizza and VonderHaar, 2012). Such variations should also be observed in sediments on the Lord Howe Rise, if the sediment was deposited continuously.

Although there are several deviations, our $^{187}Os/^{188}Os_i$ data generally display trends similar to those of the global reference curve, i.e., lower values around the silicified interval in Section 208-33R-1 (Fig. 3). The lowest $^{187}Os/^{188}Os_i$ value of 0.12±0.4 and 0.16±0.4 (2 S.D., duplicate analysis) in the siliceous claystone at 576.80-576.83 mbsf (= 208-33R-1, 80-83 cm) (Figs. 3 and 4) corresponds to the $^{187}Os/^{188}Os$ value of ~0.15 for the K-Pg boundary at Site 577 (Ravizza and Peucker-Ehrenbrink, 2003) and Site 569 (Ravizza and VonderHaar 2012). The position of this sample is at the base of the silicified interval. Modelling of the post-impact recovery of seawater Os isotopic composition indicates that the low $^{187}Os/^{188}Os$ values (<0.2) were maintained for less than 80 k.y. under various seawater Os enrichment factors with an Os residence time of 40 k.y. (Ravizza and VonderHaar, 2012). The concentration of Os, on the other hand, shows no clear peak in the siliceous claystone sample with the lowest $^{187}Os/^{188}Os_i$ value (Figs. 3 and 4), which is also characterized by a low Os concentration of 72.8-75.5 pg g^{-1}. These observations suggest that the siliceous claystone sample at 576.80-576.83 mbsf was deposited shortly after the Chicxulub impact event when the seawater $^{187}Os/^{188}Os$ value was still low, but the peak in Os concentration is missed due to a minor hiatus. The presence of minor paraconformities has been suggested within the silicified interval (Edwards, 1973a,b) and is consistent with the decrease in sedimentation rate for the silicified interval (Fig. 5).

The reference curve for marine $^{187}Os/^{188}Os$ values also captures a decreasing trend (gray line in Fig. 3) in response to the weathering of Deccan Traps flood basalt that started around the boundary between Chrons C30n and C29r (Ravizza and Peucker-Ehrenbrink, 2003; Robinson et al., 2009; Schoene et al., 2019). Our $^{187}Os/^{188}Os_i$ data show a similar trend, but some of the Maastrichtian sediment samples have lower $^{187}Os/^{188}Os_i$ values than the global $^{187}Os/^{188}Os$ trends (Fig. 3). This suggests a temporary input of nonradiogenic Os from a local or regional source into the Lord Howe Rise sediments at this time. We speculate that the source of this unradiogenic Os was either local magmatic activity on the Lord Howe Rise or regional magmatism associated with the broader tectonic evolution of Zealandia and surrounds (e.g. Mortimer and Scott, 2020). The rest of these samples, on the other hand, plot along the global reference curve for the Maastrichtian. This suggests that the overall trend of seawater Os isotopic composition on the Lord Howe Rise reflects the global ocean water $^{187}Os/^{188}Os$ values (Fig. 3), which show a gradual decrease in response to the weathering of the Deccan Traps flood basalt just before the K-Pg boundary (Ravizza and Peucker-Ehrenbrink, 2003; Robinson et al., 2009; Schoene et al., 2019).

The two samples in the silicified interval from 576.5 mbsf to 576.6 mbsf (208-33R-1, 57.5-58 cm and 51-53 cm) that have high $^{187}Os/^{188}Os_i$ values of 1.19 and 0.91 are difficult to explain (Figs. 3-4; DR1: Table S4). One possibility for the exceptionally high $^{187}Os/^{188}Os_i$ values is an increased supply of radiogenic Os from older continental crust. XRF core scanning data (Fig. 6) show slight increases in K, Ti, and Fe intensities, which may reflect the enhanced supply of terrigenous material from the surrounding continents (Australia, Zealandia) during this time interval.

Stratigraphy around the K-Pg Boundary

Three calcareous nannofossil biozones that span the K-Pg boundary are identified within Section 208-33R-1: Maastrichtian Zone UC20c-d below 576.86 mbsf (208-33R-1, 86 cm); Danian Zone CNP1/NP1 at 576.36-576.74 mbsf (208-33R-1, 36-74 cm); and Danian Zone CNP2/NP2 above 576.32 mbsf (208-33R-1, 32 cm) (Fig. 4). The biostratigraphic K-Pg boundary is located between 576.86 mbsf and 576.74 mbsf, which corresponds to the basal part of the silicified interval and to a sudden drop in calcareous nannofossil abundance. This depth is 30 cm lower than the previous K-Pg boundary estimate based on the calcareous nannofossils (Edwards, 1973a). Our interpretation is consistent with that of Hollis (1993), who investigated radiolarian biostratigraphy around the K-Pg boundary at Site 208, and predicted that the K-Pg boundary is located at the base of the silicified interval (576.8 mbsf). The $\delta^{13}C_{carb}$ data are also consistent with our calcareous nannofossil biostratigraphy, as they show a negative shift in the silicified interval in Section 208-33R-1 that is comparable to the widely recognized $\delta^{13}C_{carb}$ excursion at the K-Pg boundary.

The $^{187}Os/^{188}Os_i$ values show trends similar to those of coeval global seawater, with the minimum value of 0.12-0.16 at 576.80-576.83 mbsf, which is the base of the silicified interval. The nonradiogenic $^{187}Os/^{188}Os_i$ values correspond to the widely recognized values of the K-Pg boundary (e.g., Ravizza and Peucker-Ehrenbrink, 2003; Robinson et al., 2009; Ravizza and VonderHaar 2012). However, the concentration of Os in the K-Pg sample does not show a clear peak. As discussed above, this may indicate that the basal siliceous claystone was deposited shortly after the Chicxulub impact event, when seawater $^{187}Os/^{188}Os$ was still low, but the peak in concentration of Os was missed due to a minor hiatus. Hollis (1993) also proposed a hiatus at the base of the siliceous interval (576.8 mbsf) based on the absence of the earliest Paleocene radiolarian zone RP1 (*Amphisphaero aotea*) (Fig. S2).

The paleomagnetic record in Section 208-33R-1 (576.0-577.0 mbsf) is partly inconsistent with our bio/chemostratigraphic records (e.g., calcareous nannofossils, $\delta^{13}C_{carb}$, and $^{187}Os/^{188}Os_i$). Our new paleomagnetic data show that a normal polarity zone, correlated to Chron C29n, extends down to 576.89 mbsf (208-33R-1, 89 cm). In addition, the siliceous claystone sample at 576.74-576.83 mbsf, which we consider to be closest to the K-Pg boundary, is located within Chron C29n, rather than C29r, as should be the case for the K-Pg boundary (Fig. 4). A potential explanation for this discrepancy is that the extremely low sedimentation rate and the minor hiatus caused a delay in the burial and acquisition of magnetization lock-in. The conditions resulting in the very low sedimentation rate lasted until around the onset of C29n (65.688 Ma). After the onset of C29n, the siliceous claystone at the base of the silicified interval and the chalk just below the siliceous claystone acquired their magnetization. Another possibility is that the diagenetic formation of hematite has modified the paleomagnetic record. Samples correlated to the lower part of C29n are characterized by higher coercivity and remanence intensity (Table S3 and Fig. S1), which possibly indicates the diagenetic formation of hematite. In pelagic limestone, Channell et al. (1982) argued that hematite formation occurred after burial of 30-60 cm, while detrital magnetite acquire remanence typically at 0-15 cm depth (e.g., Suganuma et al., 2010; Horiuchi et al., 2016; Sakuramoto et al., 2017). This may explain a shift downward of the magnetization, with the base of Chron C29n potentially shifting downward by ~20-50 cm compared to the other chron boundaries.

In summary, our new data indicate that during the Maastrichtian (below 576.83 mbsf), nannofossil chalk was deposited relatively continuously. Following the K-Pg impact, production of calcifying marine phytoplankton was suddenly decimated. The reduced sedimentation rates and bottom currents may have resulted in a minor hiatus at this time. The siliceous claystone sample at 576.74-576.83 mbsf at the base of the silicified interval (208-33R-1, 74-83 cm) was deposited immediately after the K-Pg impact when the seawater $^{187}Os/^{188}Os$ value was still low (<0.2). The production and accumulation of calcifying marine phytoplankton remained very low immediately after the K-Pg impact and resulted in the very low sedimentation rates in the silicified interval (576.0-576.8 mbsf). The silicified interval itself likely reflects increased production and accumulation of biogenic silica. Dumitrica (1973) reported that radiolarians are relatively well-preserved in the silicified interval at Site 208. Enhanced production of siliceous plankton (diatom and radiolaria) has also been reported in the earliest Paleocene section of the Marlborough sub-basin in New Zealand (Hollis, 1993. 2003; Hollis et al., 1995; Taylor et al., 2018). The increased production of siliceous plankton groups may reflect regional phenomena around Zealandia (e.g., Marlborough sub-basin and the Lord Howe Rise in Fig. 1) over the first 1 m.y. of the Paleocene, when the calcareous plankton groups were decimated in diversity and abundance.

CONCLUSIONS

In this study we have examined the stratigraphy around the K-Pg boundary at DSDP Site 208 on the Lord Howe Rise using calcareous nannofossils, magnetic polarity, $\delta^{13}C_{carb}$, Os concentration and $^{187}Os/^{188}Os_i$ composition of sediment. Calcareous nannofossil biostratigraphy suggests nearly continuous sedimentation from the mid-Maastrichtian to lowermost Thanetian. Paleomagnetic reversals are also consistent with the calcareous nannofossil biostratigraphy. The resulting age model indicates average sedimentation rates of 4-5 m m.y.$^{-1}$ through the interval investigated. The calcareous nannofossil biostratigraphy indicates that the K-Pg boundary is located at a siliceous claystone (576.74-576.83 mbsf) at the base of the silicified interval in 208-33R-1 (0-83 cm). This level is slightly deeper than the previously identified K-Pg boundary (Edwards, 1973a, 1973b) and corresponds to the lithologic change from chalk to siliceous claystone and to the sudden decline in the abundance of calcareous nannofossils. The $\delta^{13}C_{carb}$ data show a clear negative shift in the silicified interval, which is consistent with the global pattern of $\delta^{13}C_{carb}$ across the K-Pg boundary. Our $^{187}Os/^{188}Os_i$ data show similar trends to those of the coeval ocean water, with the lowest $^{187}Os/^{188}Os_i$ value of 0.12-0.16 in the siliceous claystone sample, which corresponds to the biostratigraphic K-Pg boundary. However, the concentration of Os is low (<80 pg g^{-1}) in this sample, which suggests that the siliceous claystone was deposited near but not at the K-Pg boundary. This suggests that a minor hiatus may be present in the boundary interval.

This new stratigraphic data around the K-Pg boundary at DSDP Site 208 provides crucial information for regional correlation of the K-Pg strata around the circum-Australian ocean basins and plateaus (Fig. 1). The earliest Paleocene hiatuses are evident in the sediment recovered from Site 1172D in the Tasman Basin (Shipboard Scientific Party, 2001; Schellenberg et al., 2004) and in the outer shelf (Branch Stream)/upper slope (Woodside Creek) sections in the Marlborough sub-basin in New Zealand (Hollis, 2003), both of which have been attributed to an eustatic sea-level fall. Those hiatuses could be correlated to the minor hiatus at the depth of 576.8 mbsf in the sediment from Site 208, but given the deep-sea depositional setting of Site

208, it is likely that the hiatus at Site 208 developed under the presence of erosive bottom currents on the Lord Howe Rise. In contrast, the K-Pg succession recovered at Site U1514C could be more complete, because a peak in platinum group elements (including osmium) and a decrease in $^{187}Os/^{188}Os$, which are evidence of the effects of the Chicxulub impact event, have been reported but not yet analyzed in detail (Ota et al., 2020). The results presented in this study will also complement new information from Site U1514C. In 2017, IODP Expedition 371 recovered Paleocene and Upper Cretaceous sediments at Site U1509 on the southeastern Lord Howe Rise (Fig. 1) (Sutherland et al., 2019). The stratigraphy of the K-Pg boundary at Site U1509 has not yet been established because of the limited occurrence of microfossils in the Upper Cretaceous interval. The stratigraphic data for Site 208 reported in this study may help to constrain the K-Pg boundary at Site U1509 by allowing detailed stratigraphic correlations between the two sites.

ACKNOWLEDGMENTS

We thank K. Suzuki, T. Nozaki, and Y. Ohtsuki (JAMSTEC) for laboratory assistance with Re-Os analysis, H. Suga (JAMSTEC) for $\delta^{13}C_{carb}$ analysis, and T. Matsuzaki (Kochi Core Center, Kochi University) for ITRAX measurements. Merrie-Ellen Gunning provided constructive comments on an early version of the manuscript. We thank two anonymous reviewers for their helpful comments. This research used samples provided by the International Ocean Discovery Program (IODP) (Sample request numbers IODP037363, IODP058112, and IODP440531). This study was financially supported by the Japan Society for the Promotion of Science (JSPS) KAKENHI (grants 19K04054, 19H02011, 17K05674, and 17K05689). R. Hackney publishes with the permission of the chief executive officer of Geoscience Australia.

REFERENCES CITED

Agnini, C., Fornaciari, E., Raffi, I., Catanzariti, R., Pälike, H., Backman, J., and Rio, D., 2014, Biozonation and biochronology of Paleogene calcareous nannofossils from low and middle latitudes: Newsletters on Stratigraphy, v. 47, no. 2, p. 131–181, doi: 10.1127/0078-0421/2014/0042.

Alvarez, L.W., Alvarez, W., Asaro, F., and Michel, H.V., 1980, Extraterrestrial cause for the Cretaceous-Tertiary extinction: Science, v. 208, p. 1095-1108.

Barnet, J.S.K., Littler, K., Westerhold, T., Kroon, D., Leng, M.J., Bailey, I., Röhl, U., and Zachos, J.C., 2019, A high-fidelity benthic stable isotope record of late Cretaceous-early Eocene climate change and carbon-cycling: Paleoceanography and Paleoclimatology, v. 34, 672–691. https://doi.org/10.1029/2019PA003556

Bown, P.R., 1998, Calcareous nannofossil biostratigraphy: British Micropalaeontological Society Series. London: Chapman and Hall/Kluwer Academic Publishers, 315 p.

Bown, P.R., and Young, J.R., 1998, Techniques, *in* Bown, P.R., ed., Calcareous nannofossil biostratigraphy: British Micropalaeontological Society Series. London: Chapman and Hall/Kluwer Academic Publishers, p. 16–28.

Bralower, T.J., Cosmidis, J., Heaney, P.J., Kump, L.R., Morgan, J.V., Harper, D.T., Lyons, S.L., Freeman, K.H., Grice K., Wendler, J.E., Zachos, J.C., Artemieva, N., Chen, S.A., Gulick, S.P.S., House, C.H., Jones, H.L., Lowery, C.M., Nims, C., Schaefer, B., Thomas, E., and Vajda, V., 2020, Origin of a global carbonate layer deposited in the aftermath of the Cretaceous-Paleogene boundary impact: Earth and Planetary Science Letters, v. 548, 116476, https://doi.org/10.1016/j.epsl.2020.116476.

Burnett, J., 1998, Upper Cretaceous, *in* Bown, P.R., ed., Calcareous nannofossil biostratigraphy:

British Micropalaeontological Society Series. London: Chapman and Hall/Kluwer Academic Publishers, p. 132–199.

Burton, K.W., Bourdon, B., Birck, J.-L., Allègre, C.J., and Hein, J.R., 1999, Osmium isotope variations in the oceans recorded by Fe-Mn crusts: Earth and Planetary Science Letters, v. 171, p. 185-197.

Channell, J.E.T., Freeman, R., Heller, F., and Lowrie, W., 1982, Timing of diagenetic haematite growth in red pelagic limestones from Gubbio (Italy): Earth and Planetary Science Letters, v. 58, no. 2, p. 189-201, https://doi.org/10.1016/0012-821X(82)90193-5.

Cohen, A.S., and Waters, G.G., 1996, Separation of osmium from geological materials by solvent extraction for analysis by thermal ionization mass spectrometry: Analytica Chimica Acta, v. 332, p. 269–275.

Coxall, H.K., D'Hondt, S., and Zachos, J.C., 2006, Pelagic evolution andenvironmental recovery after the Cretaceous-Paleogene mass extinction: Geology, v. 34, no. 4, p. 297–300, doi:10.1130/G21702.1.

Crawford, A., Meffre, S., and Symonds, P., 2003, 120 to 0 Ma tectonic evolution of the southwest Pacific and analogous geological evolution of the 600 to 220 Ma Tasman Fold Belt System, *in* Hillis, R.R., and Müller, R.D., eds., Evolution and Dynamics of the Australian Plate: Geological Society of America Special Papers 372, p. 383-403, doi: https://doi.org/10.1130/0-8137-2372-8.383.

Croudace, I.W., Rindby, A., and Rothwell, R.G., 2006, ITRAX: description and evaluation of a new multi-function X-ray core scanner, *in* Rothwell, R.G., ed., New Techniques in Sediment Core Analysis: Geological Society, London, Special Publication 267, p. 51–63.

D'Hondt, S., Donaghay, P., Zachos, J.C., Luttenberg, D., and Lindinger, M., 1998, Organic carbon fluxes and ecological recovery from the Cretaceous-Tertiary mass extinction: Science, v. 282, no. 5387, p. 276–279, https://doi.org/10.1126/science.282.5387.276.

Dumitrica, P., 1973, Paleocene radiolaria, DSDP Leg 21, *in* Burns, R.E., Andrews, J.E., et al., Initial Reports of the Deep Sea Drilling Project, Volume 21: Washington, D.C., U.S. Government Printing Office, p. 787-817, doi:10.2973/dsdp.proc.21.124.1973.

Edwards, A.R., 1973a, Calcareous nannofossil from the Southwest Pacific, Deep Sea Drilling Project, Leg 21, *in* Burns, R.E., Andrews, J.E., et al., Initial Reports of the Deep Sea Drilling Project, Volume 21: Washington, D.C., U.S. Government Printing Office, p. 641-691, doi:10.2973/dsdp.proc.21.118.1973.

Edwards, A.R., 1973b, Southwest Pacific regional unconformities encountered during Leg 21, *in* Burns, R.E., Andrews, J.E., et al., Initial Reports of the Deep Sea Drilling Project, Volume 21: Washington, D.C., U.S. Government Printing Office, p. 701-720, doi:10.2973/dsdp.proc.21.120.1973.

Gradstein, F.M., Ogg, J.G., Schmitz, M.D., and Ogg, G.M., 2020, The Geologic Time Scale 2020: Amsterdam, Elsevier B.V.

Hollis, C.J., 1993, Latest Cretaceous to Late Paleocene radiolarian biostratigraphy: A new zonation from the New Zealand region: Marine Micropaleontology, v. 21, p. 295-327.

Hollis, C.J., 2003, The Cretaceous/Tertiary boundary event in New Zealand: profiling mass extinction: New Zealand Journal of Geology and Geophysics, v. 46, p. 307–321.

Hollis, C.J., Rodgers, K.A., and Parker, R.J., 1995, Siliceous plankton bloom in the earliest Tertiary of Marlborough, New Zealand: Geology, v. 23, p. 835–838.

Horiuchi, K, Kamata, K., Maejima, S., Sasaki, S., Sasaki, N., Yamazaki, T., Fujita, S., Motoyama, H., and Matsuzaki, H., 2016, Multiple ^{10}Be records revealing the history of cosmic-ray variations across the Iceland Basin excursion: Earth and Planetary Science Letters, v. 440, p. 105-114, https://doi.org/10.1016/j.epsl.2016.01.034.

Hsiung, K.-H., Kanamatsu, T., Ikehara, K., Usami, K., Horng, C.-S., Ohkouchi, N., Ogawa, N.O., Saito, S., and Murayama, M., 2021, X-ray fluorescence core scanning, magnetic signatures, and organic geochemistry analyses of Ryukyu Trench sediments: turbidites and hemipelagites: Progress in Earth and Planetary Science, v. 8, no. 2, https://doi.org/10.1186/s40645-020-00396-2

Huber, B.T., Hobbs, R.W., Bogus, K.A., et al., 2019, Site U1514, *in* Hobbs, R.W., Huber, B.T., Bogus, K.A., and the Expedition 369 Scientists, Australia Cretaceous Climate and Tectonics, Proceedings of the International Ocean Discovery Program, Volume 369: College Station, Texas, International Ocean Discovery Program, https://doi.org/10.14379/iodp.proc.369.105.2019.

Hull, P.M., Bornemann, A., Penman, D.E., Henehan, M.J. Norris, R.D., Wilson, P.A., Blum, P., Alegret, L., Batenburg, S.J., Bown, P.R., Bralower, T.J., Cournede, C., Deutsch, A., Donner, B., Friedrich, O., Jehle, S., Kim, H., Kroon, D., Lippert, P.C., Loroch, D., Moebius, I., Moriya, K., Peppe, D.J., Ravizza, G.E., Röhl, U., Schueth, J.D., Sepúlveda, J., Sexton, P.F., Sibert, E.C., Śliwińska, K.K., Summons, R.E., Ellen Thomas, E., Thomas Westerhold, T., Whiteside, J.H., Yamaguchi, T., and Zachos, J.C., 2020, On impact and volcanism across the Cretaceous-Paleogene boundary: Science, v. 367, no. 6475, p. 266-272, doi: 10.1126/science.aay5055.

Kirschvink, J.L., 1980, The least-squares line and plane and the analysis of palaeomagnetic data: Geophysical Journal of the Royal Astronomical Society, v. 62, no. 3, p. 699-718.

Kroon, D., Zachos, J.C., and Leg 208 Scientific Party, 2007, Leg 208 synthesis: Cenozoic climate cycles and excursions, *in* Kroon, D., Zachos, J.C., and Richter, C., Proceedings of the Ocean Drilling Program, Scientific Results, Volume 208: College Station, Texas, Ocean Drilling Program, p. 1–55, https://doi.org/10.2973/odp.proc.sr.208.201.2007.

Kuroda, J., Hori, R.S., Suzuki, K., Gröcke, D.R., and Ohkouchi, N., 2010, Marine osmium isotope record across the Triassic-Jurassic boundary from a Pacific pelagic site: Geology, vol. 38, p. 1095-1098, doi: 10.1130/G31223.1.

Levasseur, S., Birck, J.-L., and Allègre, C.J., 1999, The osmium riverine flux and the oceanic mass balance of osmium: Earth and Planetary Science Letters, v. 174, p. 7-23, doi:10.1016/S0012-821X(99)00259-9.

Lurcock, P.C., and Wilson, G.S., 2012, PuffinPlot: A versatile, user-friendly program for paleomagnetic analysis: Geochemistry, Geophysics, Geosystems, v. 13, Q06Z45, doi:10.1029/2012GC004098.

Martini, E., 1971, Standard Tertiary and Quaternary calcareous nannoplankton zonation, *in* Farinacci, A., ed., Proceedings of the Second International Conference on Planktonic Microfossils Roma: Rome, Ed. Tecnosci., v. 2, p. 739–785.

Mortimer, N., and Scott, J.M., 2019, Volcanoes of Zealandia and the Southwest Pacific: New Zealand Journal of Geology and Geophysics, v. 63, no. 1, p. 371-377, https://doi.org/10.1080/00288306.2020.1713824.

Müller, R.D., Sdrolias, M., Gaina, C., and Roest, W.R., 2008, Age, spreading rates, and spreading asymmetry of the world's ocean crust: Geochemistry, Geophysics, Geosystems, v. 9, no. 4, Q04006, http://dx.doi.org/10.1029/2007GC001743.

Ogg, J.G., 2020, Geomagnetic Polarity Time Scale, *in* Gradstein, F.M., Ogg, J.G., Schmitz, M.D, and Ogg, G.M., eds., The Geologic Time Scale 2020: Amsterdam, Elsevier B.V., p. 159–

192.

Ota, H., Kuroda, J., Tejada, M.L.G. and IOPD Exp 369 Shipboard Science Party, 2020, Osmium isotopic composition and platinum group element abundances of Cretaceous-Paleogene boundary section at Site U1514C on the Mentelle Basin, SW Australia: Abstract MIS11-P03 presented at JPGU-AGU Joint Meeting 2020.

Oxburgh, R., 2001, Residence time of osmium in the oceans: Geochemistry, Geophysics, Geosystems, v. 2, paper no. 2000GC000104.

Pearson, D.G., and Woodland, S.J., 2000, Solvent extraction/anion exchange separation and determination of PGEs (Os, Ir, Pt, Pd, Ru) and Re-Os isotopes in geological samples by isotope dilution ICP-MS: Chemical Geology, v. 165, p. 57-107.

Peucker-Ehrenbrink, B., and Ravizza, G., 2000, The marine osmium isotopic record: Terra Nova, v. 12, p. 205-219.

Ravizza, G., and Peucker-Ehrenbrink, B., 2003, Chemostratigraphic evidence of Deccan volcanism from the marine osmium isotope record: Science, v. 302, p. 1392–1395.

Ravizza, G., and VonderHaar, D., 2012, A geochemical clock in earliest Paleogene pelagic carbonates based on the impact-induced Os isotope excursion at the Cretaceous-Paleogene boundary: Paleoceanography, v. 27, PA3219, doi:10.1029/2012PA002301.

Robinson, N., Ravizza G., Coccioni, R., Peucker-Ehrenbrink, B., and Norris, R., 2009, A high-resolution marine $^{187}Os/^{188}Os$ record for the late Maastrichtian: distinguishing the chemical fingerprints of Deccan volcanism and the KP impact event: Earth and Planetary Science Letters, v. 281, p. 159–168, doi: 10.1016/j.epsl.2009.02.019.

Rocchia, R., Boclet, D., Bonté, P., Froget, L., Galbrun, B., Jéhanno, C., and Robin, E., 1992, Iridium and other element distributions, mineralogy, and stratigraphy near the

Cretaceous/Tertiary boundary in Hole 761C, *in* von Rad, U., Haq, B.U., et al., Proceedings of the Ocean Drilling Program, Scientific Results, Volume 122: College Station, Texas, USA, Ocean Drilling Program, p. 753-762,

Roy-Barman, M., 1993, Mesure du rapport $^{187}Os/^{188}Os$ dans les basaltes et les péridotites. Contribution à la systematique ^{187}Re-^{187}Os dans le manteau [Ph.D. thesis]: Univ. de Paris VII, Paris.

Sakuramoto, Y., Yamazaki, T., Kimoto, K., Miyairi, Y., Kuroda, J., Yokoyama, Y., and Matsuzaki, H., 2017, A geomagnetic paleointensity record of 0.6 to 3.2 Ma from sediments in the western equatorial Pacific and remanent magnetization lock-in depth: Journal of Geophysical Research: Solid Earth, v. 122, p. 7525-7543, https://doi.org/10.1002/2017JB014450.

Schellenberg, S.A., Brinkhuis, H., Stickley, C.E., Fuller, M., Kyte, F.T., and Williams, G.L., 2004, The Cretaceous/Paleogene transition on the East Tasman Plateau, southwestern Pacific, *in* Exon, N.F., Kennett, J.P., and Malone, M.J., eds., The Cenozoic Southern Ocean: Tectonics, Sedimentation, and Climate Change Between Australia and Antarctica, Geophys. Monogr. Ser., vol. 151, pp. 93-112, AGU, Washington, D. C.

Schoene, B., Eddy, M.P., Samperton, K.M., Keller, C.B., Keller, G., Adatte, T., and Khadri, S.F.R., 2019, U-Pb constraints on pulsed eruption of the Deccan Traps across the end-Cretaceous mass extinction: Science, v. 363, no. 6429, p. 862–866, doi: 10.1126/science.aau2422.

Schulte, P., Alegret, L., Arenillas, I., Arz, J.A., Barton, P.J., Bown, P.R., Bralower, T.J., Christeson, G.L., Claeys, P., Cockell, C.S., Collins, G.S., Deutsch, A., Goldin, T.J., Goto, K., Grajales-Nishimura, J.M., Grieve, R.A.F., Gulick, S.P.S., Johnson, K.R., Kiessling, W., Koeberl, C., Kring, D.A., MacLeod, K.G., Matsui, T., Melosh, J., Montanari, A., Morgan, J.V., Neal, C.R., Nichols, D.J., Norris, R.D., Pierazzo, E., Ravizza, G., Rebolledo-Vieyra, M., Uwe Reimold, W., Robin, E., Salge, T., Speijer, R.P., Sweet, A.R., Urrutia-Fucugauchi, J., Vajda, V., Whalen, M.T., and Willumsen, P.S., 2010, The Chicxulub bolide impact and mass extinction at the Cretaceous-Paleogene boundary: Science, v. 327, p. 1214-1218, doi: 10.1126/science.1177265.

Seki, A., Tada, R., Kurokawa, S., and Murayama, M., 2019, High-resolution Quaternary record of marine organic carbon content in the hemipelagic sediments of the Japan Sea from bromine counts measured by XRF core scanner: Progress in Earth and Planetary Science, v. 6, no. 1, https://doi.org/10.1186/s40645-018-0244-z

Sharma, M., Papanastassiou, D.A., and Wasserburg, G.J., 1997, The concentration and isotopic composition of Os in the oceans: Geochimica et Cosmochimica Acta, v. 61, p. 3287-3299.

Shipboard Scientific Party, 1990, Site 761, *in* Haq, B.U., von Rad, U., O'Connell, S., et al., Proceedings of the Ocean Drilling Program, Initial Reports, Volume 122: College Station, Texas, Ocean Drilling Program, p. 161–211, doi:10.2973/odp.proc.ir.122.107.1990.

Shipboard Scientific Party, 1991, Site 807, *in* Kroenke, L.W., Berger, W.H., Janecek, T.R., et al., Proceedings of the Ocean Drilling Program, Initial Reports, Volume 130: College Station, Texas, Ocean Drilling Program, p. 369-493, doi:10.2973/odp.proc.ir.130.109.1991.

Shipboard Scientific Party, 2001, Site 1172, *in* Exon, N.F., Kennett, J.P., Malone, M.J., et al., Proceedings of the Ocean Drilling Program, Initial Reports, Volume 189: College

Station, Texas, Ocean Drilling Program, p. 1-149, https://doi.org/10.2973/odp.proc.ir.189.107.2001

Shirey, S.B., and Walker, R.J., 1995, Carius tube digestion for low-blank rhenium-osmium analysis: Analytical Chemistry, v. 67, p. 2136–2141.

Smoliar, M.I., Walker, R.J., and Morgan, J.W., 1996, Re-Os isotope constraints on the age of Group IIA, IIIA, IVA, and IVB iron meteorites: Science, v. 271, p. 1099–1102.

Suganuma, Y., Yokoyama, Y., Yamazaki, T., Kawamura, K., Horng, C.-S., and Matsuzaki, H., 2010, ^{10}Be evidence for delayed acquisition of remanent magnetization in marine sediments: Implication for a new age for the Matuyama–Brunhes boundary: Earth and Planetary Science Letters, v. 296, no. 3-4, p. 443-450, https://doi.org/10.1016/j.epsl.2010.05.031.

Sutherland, R., Dickens, G.R., Blum, P., and the Expedition 371 Scientists, 2019, Tasman Frontier Subduction Initiation and Paleogene Climate, Proceedings of the International Ocean Discovery Program, Volume 371: College Station, Texas, International Ocean Discovery Program, https://doi.org/10.14379/iodp.proc.371.2019

Taylor, K.W.R., Willumsen, P.S., Hollis, C.J., and Pancost, R.D., 2018, South Pacific evidence for the long-term climate impact of the Cretaceous/Paleogene boundary event: Earth-Science Reviews, v. 179, p. 287–302

Tejada, M.L.G., Suzuki, K., Kuroda, J., Coccioni, R., Mahoney, J.J., Ohkouchi, N., Sakamoto, T., and Tatsumi, Y., 2009, Ontong Java Plateau eruption as a trigger for the early Aptian oceanic anoxic event: Geology, v. 37, p. 855–858, doi: 10.1130/G25763A.1.

The Shipboard Scientific Party et al., 1973, Site 208, *in* Burns, R.E., Andrews, J.E., et al., Initial Reports of the Deep Sea Drilling Project, Volume 21: Washington, D.C., U.S.

Government Printing Office, p. 271-331 doi: 10.2973/dsdp.proc.21.108.1973.

White, L.T., Gibson, G.M., and Lister, G.S., 2013, A reassessment of paleogeographic reconstructions of eastern Gondwana: Bringing geology back into the equation: Gondwana Research, v. 24, p. 984-998, http://dx.doi.org/10.1016/j.gr.2013.06.009.

Watkins, D.K, Wise Jr., S.W., Pospichal, J.J., and Crux, J., 1996, Upper Cretaceous calcareous nannofossil biostratigraphy and paleoceanography of the Southern Ocean, *in* Moguilevsky, A., and Whatley, R., eds., Microfossils and Ocean Environments, Proceedings of the "ODP and Marine Biosphere" International Conference, Aberystwyth, 19-21 April 1994, University of Wales, Aberystwyth Press, p. 355-381.

FIGURE CAPTIONS

Figure 1.

Location of Deep Sea Drilling Project (DSDP) Site 208 on the Lord Howe Rise, southwestern Pacific, is shown. Bathymetry and tectonic boundaries are after Sutherland et al. (2019). Locations of Ocean Drilling Program (ODP) Site 1172, International Ocean Discovery Program (IODP) Site U1509, and the Marlborough sub-basin in New Zealand are also shown (see text). Wider map (inset) also shows the locations of Sites 807, 761, and U1514.

Figure 2.

Downhole profiles of cores Cores 208-29R to 208-34R at Site 208 are shown. From left to right, core recovery, scan image of split surface, epoch, stage, calcareous nannofossils (zones and bioevents), and magnetic polarity (data and expected chron) are shown. Calcareous nannofossil zones for the Upper Cretaceous are after Burnett (1998), and those for the Paleocene are after Martini (1971) and Agnini et al. (2014). PCA—Principal component analysis.

Figure 3.

Stratigraphic and geochemical records from Cores 208-33R and 208-34R are shown. From the left: core recovery, scan image of split surface, epoch, stage, calcareous nannofossil zone, magnetic polarity (data and expected Chron), and depth profiles of Os and Re concentrations, measured Os isotopic composition, age-corrected initial Os isotopic composition ($^{187}Os/^{188}Os_i$), and bulk carbonate carbon isotopic composition ($\delta^{13}C_{carb}$) are shown. The Paleocene calcareous nannofossil zones are after Martini (1971) and Agnini et al. (2014), and those of the Upper Cretaceous are after Burnett (1998). The legend for magnetic polarity data is given in Fig. 2. The light gray line in the $^{187}Os/^{188}Os_i$ panel represents the reference line of global ocean $^{187}Os/^{188}Os$ values (Ravizza and Peucker-Ehrenbrink, 2003; Robinson et al., 2009; Ravizza and VonderHaar, 2012; Hull et al., 2020). VPDB—Vienna Pee Dee Belemnite.

Figure 4.

Stratigraphic and geochemical records of Section 208-33R-1 are shown. From the left, scanned image of split section half, epoch, stage, calcareous nannofossil zone, magnetic polarity (data and expected chron), and depth profiles of Os and Re concentrations, measured $^{187}Os/^{188}Os$ and initial $^{187}Os/^{188}Os_i$ values. Paleogene calcareous nannofossil zones are after Martini (1971) and Agnini et al. (2014), and those of the Upper Cretaceous are after Burnett (1998). Gray band represents the possible position of the K-Pg boundary. Asterisk (*) indicates the previously proposed K-Pg boundary of Edwards (1973a, 1973b). The legend for magnetic polarity data is given in Fig. 2. VPDB—Vienna Pee Dee Belemnite.

Figure 5.

A depth-age plot for Site 208 is shown. Magnetic chrons, calcareous nannofossil zones, datums, and age assignments follow Gradstein et al. (2020). Paleogene calcareous nannofossil zones are after Martini (1971—NP code) and Agnini et al. (2014—CNP code), and those of the Upper Cretaceous are after Burnett (1998). The dashed line indicates the age-depth regression line used for Re-Os age correlation.

Figure 6.

X-ray fluorescence (XRF) core scanning data of Section 208-33R-1A are shown. Elemental abundances are expressed as X-ray intensity. Horizontal gray band represents possible position of the K-Pg boundary.

[1]Supplemental Material: Tables S1–S4 and Figures S1–S2. Please visit https://doi.org/10.1130/GSAB.S.XXXX to access the supplemental material, and contact editing@geosociety.org with any questions.

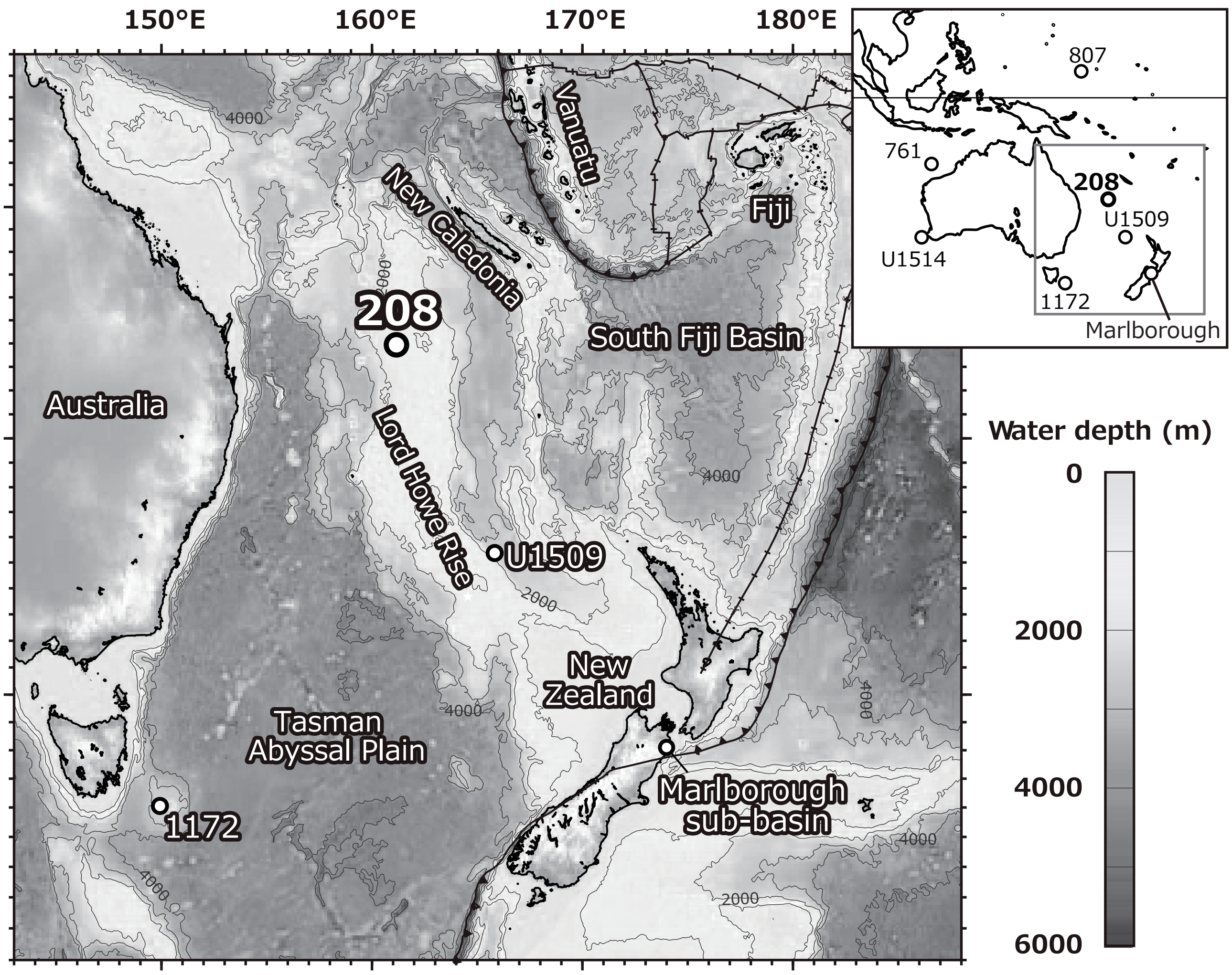
150°E
160°E
170°E
180°E
20°S
30°S
40°S
Vanuatu
New Caledonia
Fiji
208
South Fiji Basin
Australia
Lord Howe Rise
U1509
New Zealand
Tasman Abyssal Plain
Marlborough sub-basin
1172
4000
2000
807
761
U1514
Marlborough
Water depth (m)
0
2000
4000
6000

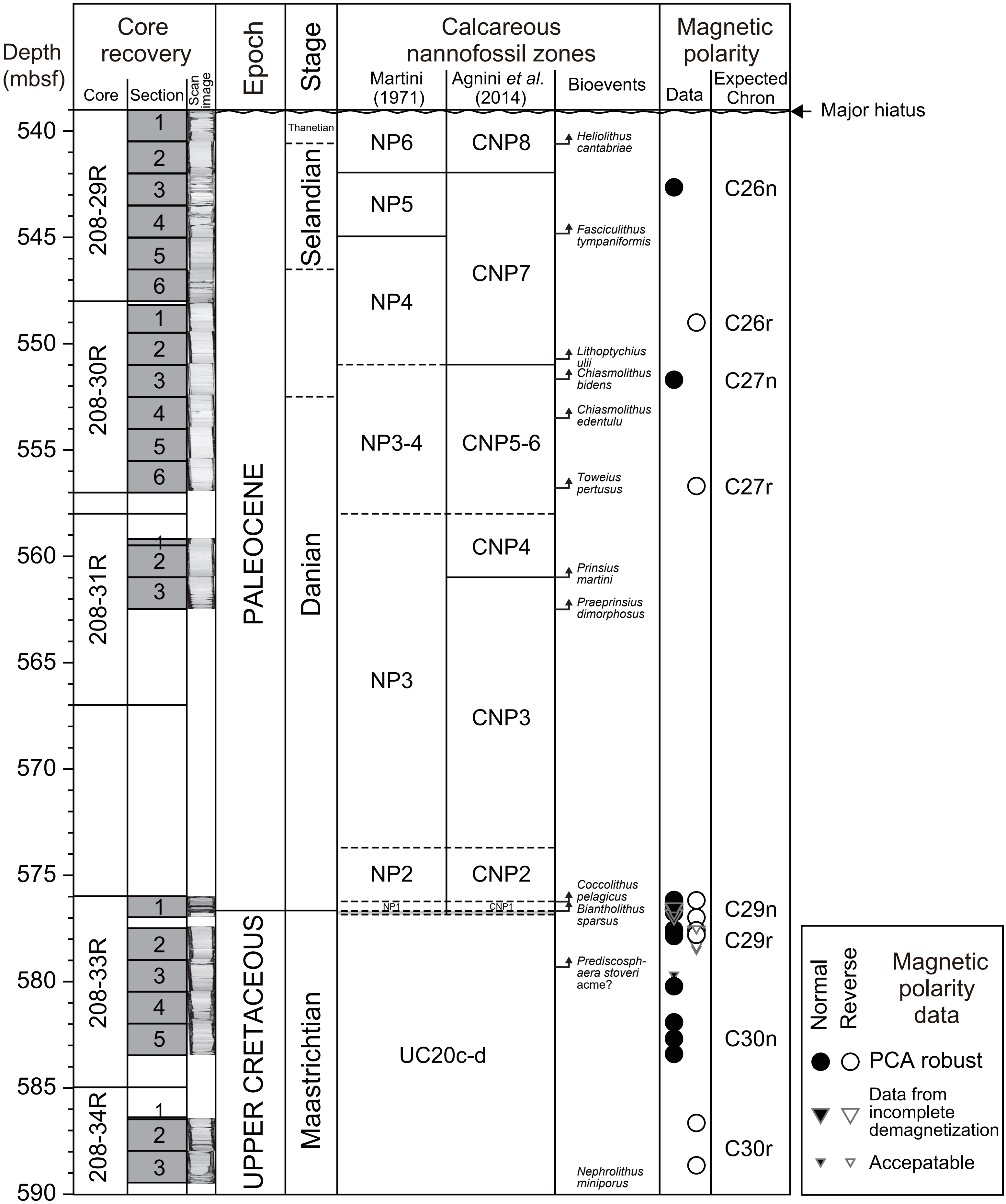

Depth (mbsf)
Core recovery
Core
Section
Scan image
Epoch
Stage
Calcareous nannofossil zones
Martini (1971)
Agnini et al. (2014)
Bioevents
Magnetic polarity
Data
Expected Chron
Major hiatus
540
545
550
555
560
565
570
575
580
585
590
208-29R
208-30R
208-31R
208-33R
208-34R
PALEOCENE
UPPER CRETACEOUS
Thanetian
Selandian
Danian
Maastrichtian
NP6
NP5
NP4
NP3-4
NP3
NP2
NP1
CNP8
CNP7
CNP5-6
CNP4
CNP3
CNP2
CNP1
UC20c-d
Heliolithus cantabriae
Fasciculithus tympaniformis
Lithoptychius ulii
Chiasmolithus bidens
Chiasmolithus edentulu
Toweius pertusus
Prinsius martini
Praeprinsius dimorphosus
Coccolithus pelagicus
Biantholithus sparsus
Prediscosph-aera stoveri acme?
Nephrolithus miniporus
C26n
C26r
C27n
C27r
C29n
C29r
C30n
C30r
Normal
Reverse
Magnetic polarity data
PCA robust
Data from incomplete demagnetization
Accepatable

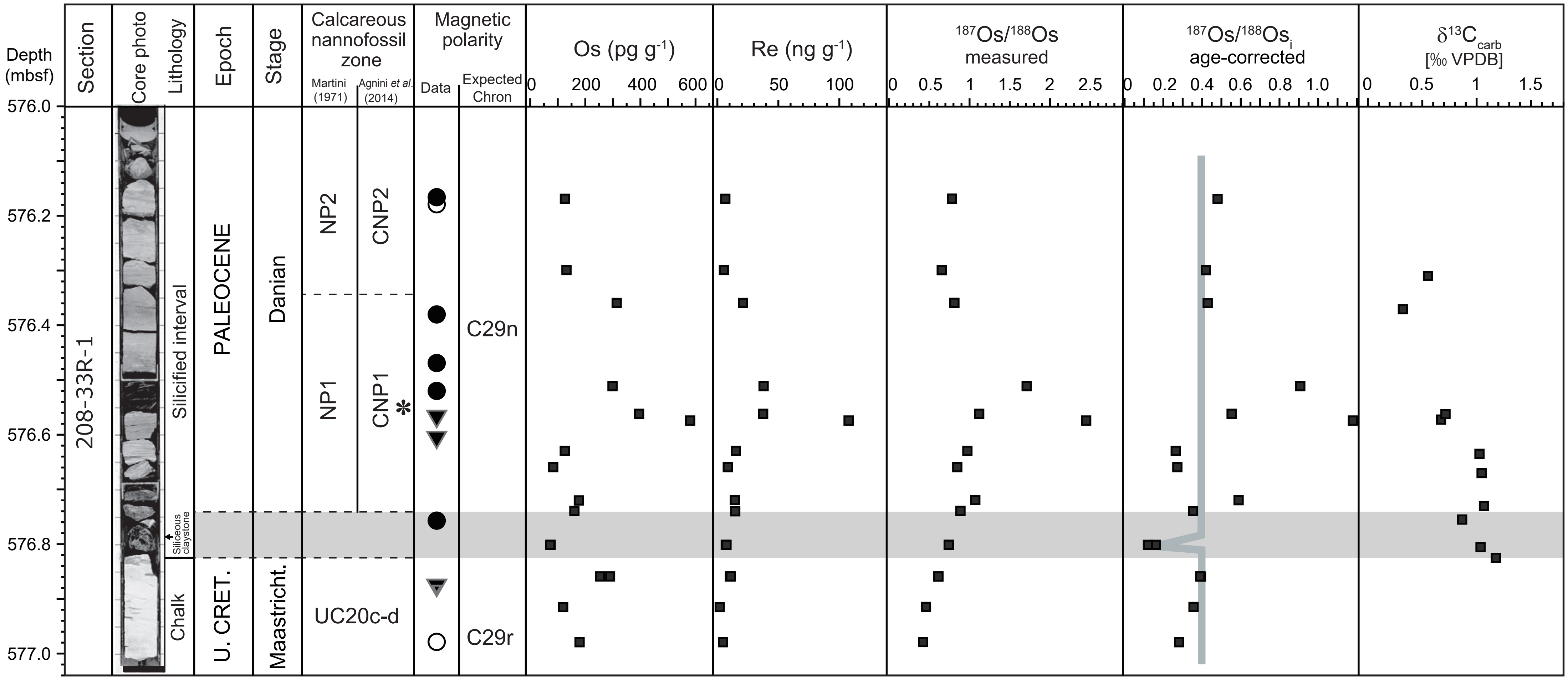

Depth (mbsf)
Section
Core photo
Lithology
Epoch
Stage
Calcareous nannofossil zone
Martini (1971)
Agnini et al. (2014)
Magnetic polarity
Data
Expected Chron
Os (pg g-1)
Re (ng g-1)
187Os/188Os measured
187Os/188Osi age-corrected
δ13Ccarb [‰ VPDB]
576.0
576.2
576.4
576.6
576.8
577.0
208-33R-1
Silicified interval
Siliceous claystone
Chalk
PALEOCENE
U. CRET.
Danian
Maastricht.
NP2
CNP2
NP1
CNP1
UC20c-d
C29n
C29r

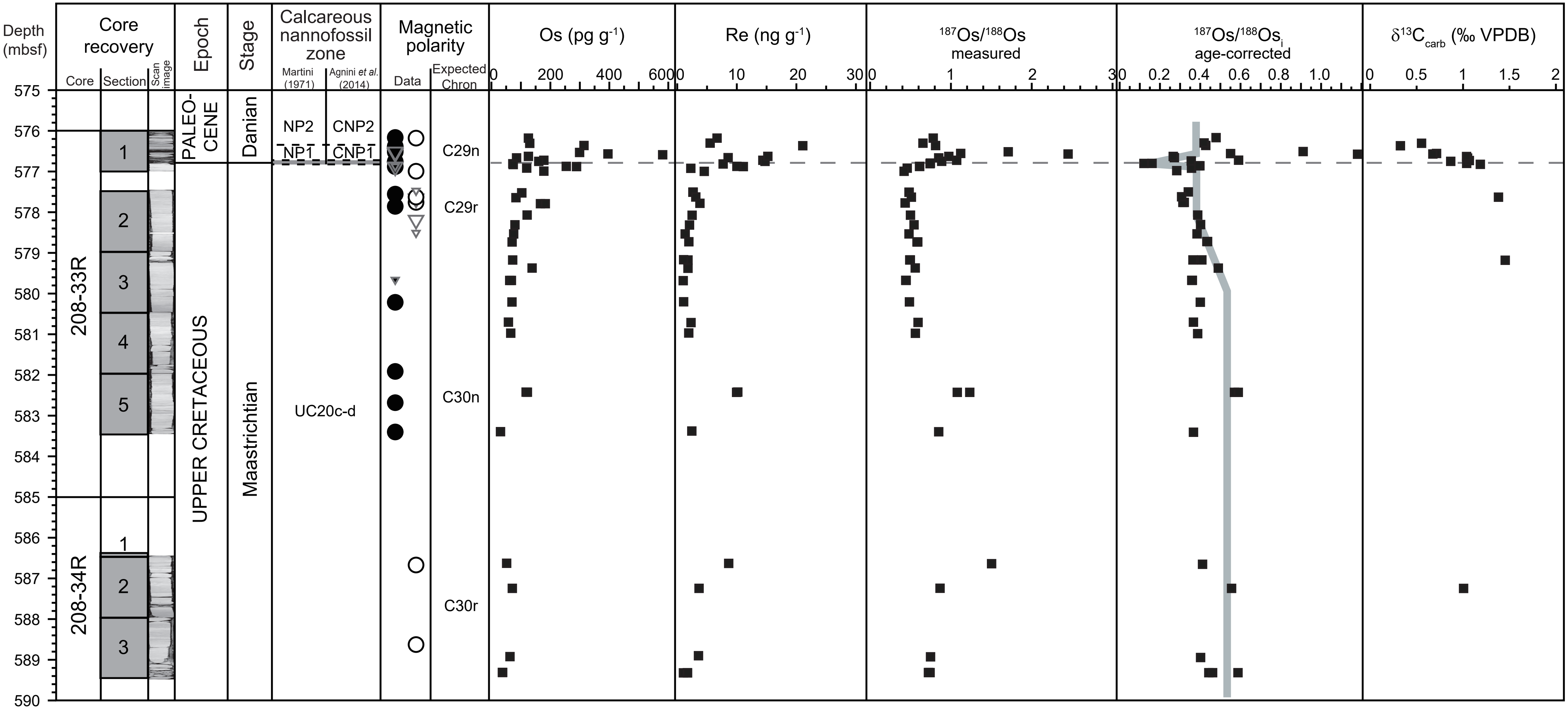

Depth (mbsf)
Core recovery
Core
Section
Scan image
Epoch
Stage
Calcareous nannofossil zone
Martini (1971)
Agnini et al. (2014)
Magnetic polarity
Data
Expected Chron
Os (pg g-1)
Re (ng g-1)
187Os/188Os measured
187Os/188Osi age-corrected
δ13Ccarb (‰ VPDB)
PALEO-CENE
UPPER CRETACEOUS
Danian
Maastrichtian
NP2
CNP2
NP1
CNP1
UC20c-d
C29n
C29r
C30n
C30r
208-33R
208-34R

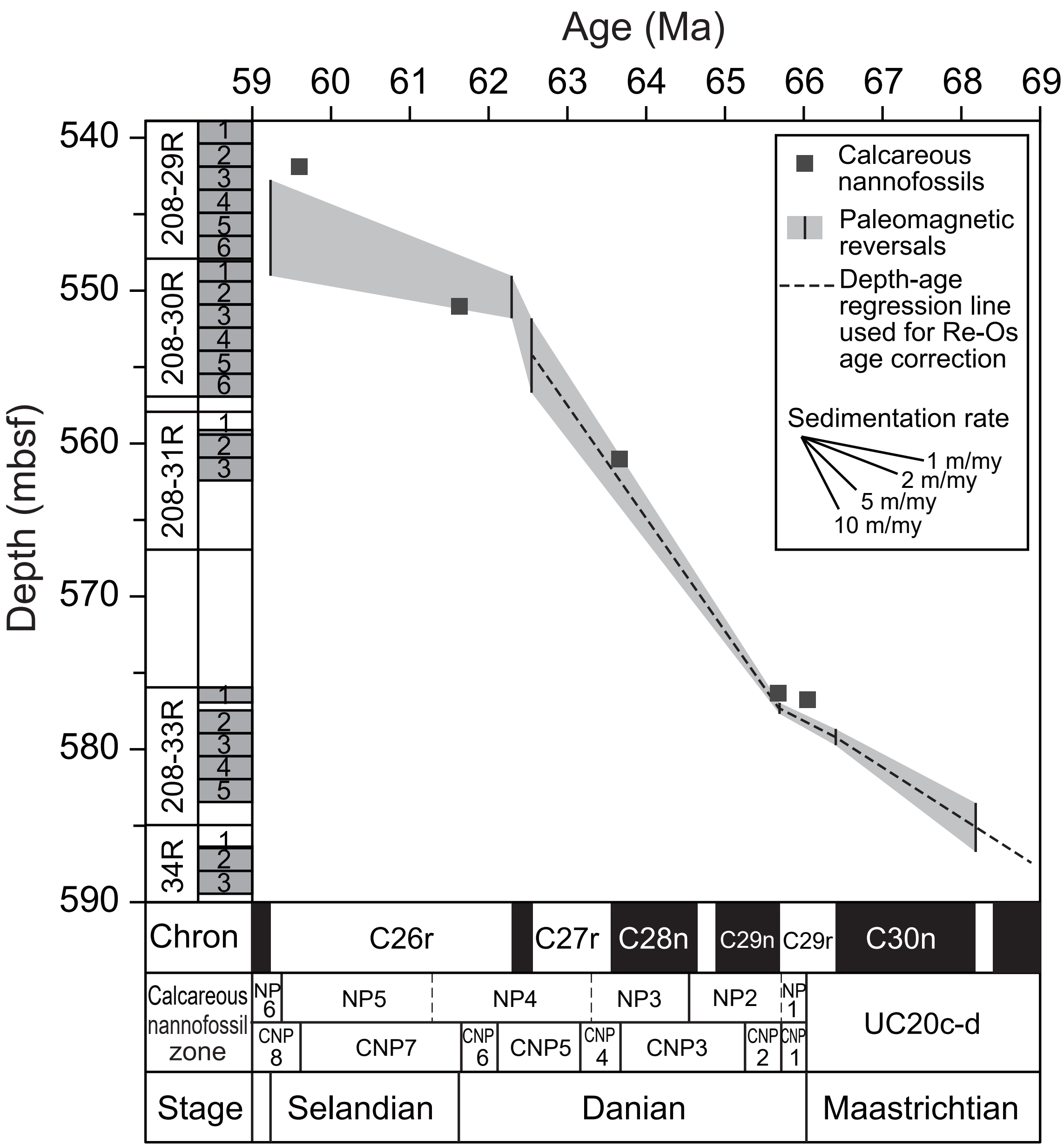

Age (Ma)
59
60
61
62
63
64
65
66
67
68
69
Depth (mbsf)
540
550
560
570
580
590
208-29R
208-30R
208-31R
208-33R
34R
Calcareous nannofossils
Paleomagnetic reversals
Depth-age regression line used for Re-Os age correction
Sedimentation rate
1 m/my
2 m/my
5 m/my
10 m/my
Chron
C26r
C27r
C28n
C29n
C29r
C30n
Calcareous nannofossil zone
NP 6
NP5
NP4
NP3
NP2
NP 1
CNP 8
CNP7
CNP 6
CNP5
CNP 4
CNP3
CNP 2
CNP 1
UC20c-d
Stage
Selandian
Danian
Maastrichtian

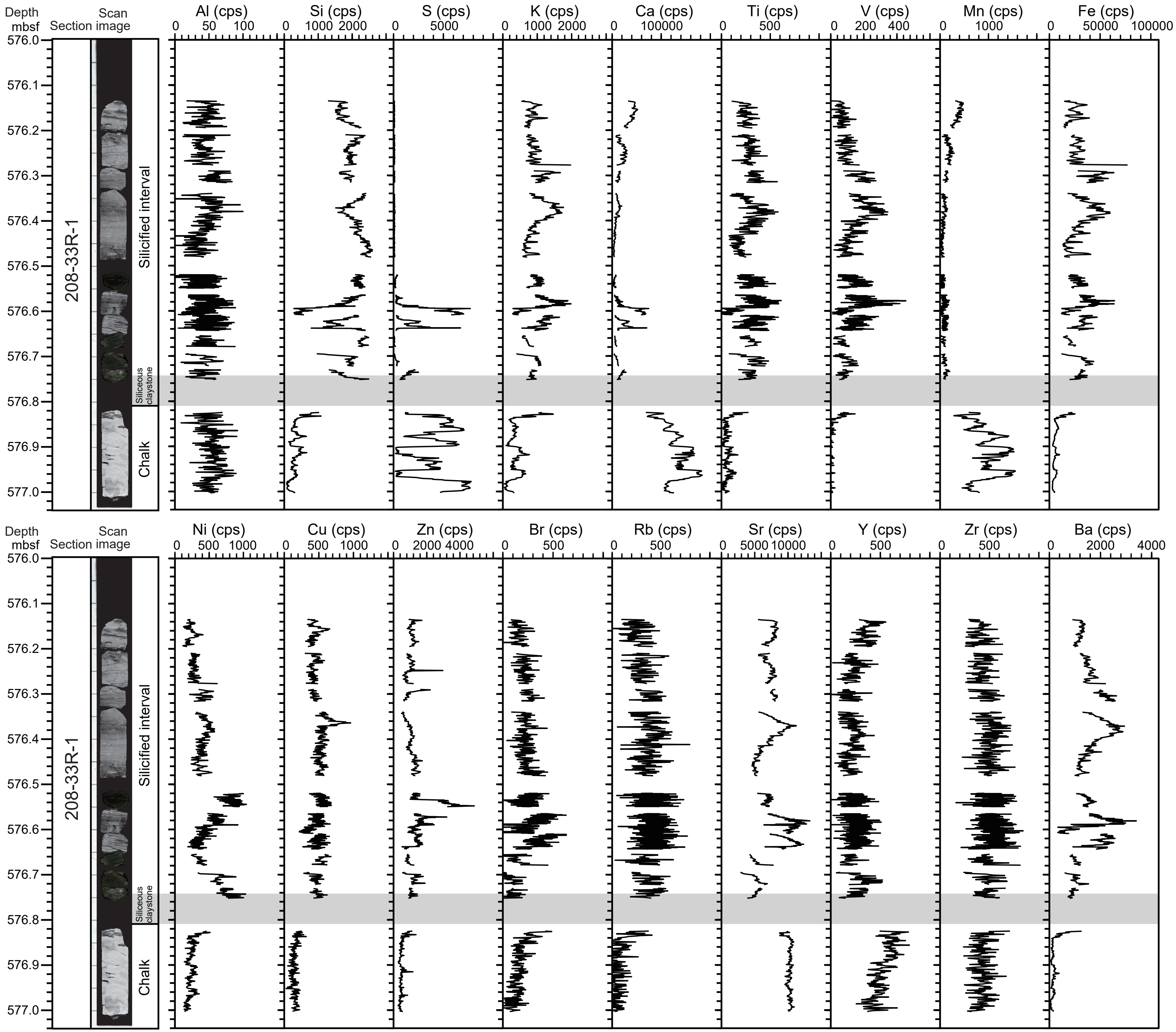

Depth mbsf
Section
Scan image
Al (cps)
Si (cps)
S (cps)
K (cps)
Ca (cps)
Ti (cps)
V (cps)
Mn (cps)
Fe (cps)
Ni (cps)
Cu (cps)
Zn (cps)
Br (cps)
Rb (cps)
Sr (cps)
Y (cps)
Zr (cps)
Ba (cps)
208-33R-1
Silicified interval
Siliceous claystone
Chalk